Journal of Power Sources 195 (2010) 8019–8027

Contents lists available at ScienceDirect

Journal of Power Sources

journal homepage: www.elsevier.com/locate/jpowsour

Comparison of ultra-fast microwave sintering and conventional thermal sintering in manufacturing of anode support solid oxide fuel cell

Zhenjun Jiao [a], Naoki Shikazono [a,*], Nobuhide Kasagi [b]

[a] Institute of Industrial Science, The University of Tokyo, 4-6-1 Komaba, Meguro-ku, Tokyo 153-8505, Japan
[b] Department of Mechanical Engineering, The University of Tokyo, Bunkyo-ku, Tokyo 113-8656, Japan

ARTICLE INFO

Article history:
Received 14 April 2010
Received in revised form 22 June 2010
Accepted 23 June 2010
Available online 30 June 2010

Keywords:
Microwave
3-D reconstruction
SOFC
TPB
Ponderomotive force

ABSTRACT

Ultra-fast microwave sintering in a multi-mode domestic microwave oven with selective susceptor and spacer has been proved to be an effective and facile method in the manufacturing of anode support solid oxide fuel cell (SOFC). Two anode support SOFCs were fabricated by using ultra-fast microwave sintering and conventional thermal sintering techniques, separately. The performances of the two cells were measured and compared in a temperature range of 700–800 °C. The microstructures of the two cells after the measurements were compared qualitatively based on SEM images. FIB-SEM technique was used to reconstruct the 3-D microstructure of both anode and cathode. The quantitative comparison of 3-D reconstructions shows the application potential and the advantages of microwave technique in SOFCs manufacturing.

1. Introduction

As one of the most promising electric power conversion systems, solid oxide fuel cell (SOFC) has been identified as an attractive efficient device for the electrochemical energy conversion in the recent few decades. SOFC working in a high-temperature environment is attracting more attention because of its fuel flexibility, high efficiency and low pollution. In order to achieve long time stability and reducing the equipment cost of the power conversion system, low temperature anode-support SOFC has been investigated by many researchers with an emphasis on reducing the thickness of electrolyte, which dominants the fuel cell resistance. As a result, anode support SOFC attracts more attention because of its high power density with very thin electrolyte [1].

The fabrication of thin film electrolyte onto anode substrate is a challenging procedure in the manufacturing of the whole cell. Zhang et al. [2] reported a novel method for fabricating thin film electrolyte. In their experimental procedures, 10 μm-thick YSZ (yttria stabilized zirconia) film was fabricated onto an anode substrate by revolving a rod at low rotation speed. Their cell shows a maximum power density of 1.4 W cm^{-2} at 800 °C. The anode substrate with thin film electrolyte is sintered at a temperature of 1400 °C, and the cathode screen-printed on the electrolyte layer is sintered at a temperature of 1200 °C. For most of the researchers, the investigations of SOFC mainly focus on electrode materials and their fabrication processes, and all the cells are sintered by the conventional heating method. Few papers were published on the new techniques for cell sintering.

Compared to the conventional sintering method which is time-and-energy consuming, some researchers have shown the possibility of using microwave for rapid sintering [3,4]. Microwave heating is a self-heating process which is accomplished by absorbing electromagnetic energy by a dielectric material. Higher heating rate and efficiency can be obtained by using microwave volumetric heating. The energy absorbed by a dielectric material per volume is estimated as $p = (1/2)\varepsilon_0\varepsilon''\omega E^2 V$ [3], where E is the electrical field strength, ω_0 is the dielectric constant in a vacuum, ε'' is the dielectric loss factor of the material, ω is the angular frequency of the external electromagnetic field and V is the material volume. At room temperature, most of the ceramics have low dielectric loss factor so that it is impossible to raise the temperature. Susceptors made by special material with large dielectric loss coefficient are needed as a pre-heater to raise temperature to the critical value beyond which the material to be sintered can be self-heated [3].

In microwave sintering process, the material volumetric heating mechanism makes the sintering process rapid and selective. Fujitsu et al. [3] successfully used microwave energy to achieve the sintering of stabilized zirconia in a 2.45-GHz multimode microwave furnace with selective susceptors. The full sintering temperature of zirconia was reduced by 100–150 °C as compared to the conventional thermal sintering, and a finer grain size was obtained. In a review of this technique, Clark [5] summarized the fundamen-

* Corresponding author.
E-mail address: shika@iis.u-tokyo.ac.jp (N. Shikazono).

0378-7753/$ – see front matter © 2010 Elsevier B.V. All rights reserved.
doi:10.1016/j.jpowsour.2010.06.072

tals, benefits, and major research issues of microwave processing of materials.

Microwave heating offers an ultra-fast method for ceramic with an ultra-large heating rate. The grain size uniformity increases because of a few orders higher densification rate in a short sintering time. Only a few groups have investigated the use of microwave sintering in manufacturing SOFC. Oh et al. [6] used GDC(gadolia doped ceria) as electrolyte and performed microwave sintering for SOFC, which clearly demonstrated the merits of microwave sintering such as lower processing temperature and rapid thermal treatment. The microwave-sintered cell exhibited higher peak power density at 650 °C compared to conventional sintered cell with the same materials. In the paper, no systematical work was introduced on the manufacturing procedures and the microstructures comparison between microwave-sintered and thermal-sintered cells. The only information which was reported is the sintering time, i.e. 1 h for anode–electrolyte co-sintering and 1 h for cathode sintering.

Details of the manufacturing procedures of both microwave-sintered and thermal-sintered SOFCs have already been introduced in our previous paper [7]. Much shorter sintering time was applied in the fabrication process, i.e. 10 min for anode–electrolyte co-sintering and 10 min for cathode sintering. In this paper, further comparison is conducted between microwave-sintered and conventional thermal-sintered cells on their performances and microstructures. With the same anode and cathode materials used, quantitative comparison of the cell performances and microstructures between microwave-sintered cell and thermal-sintered cell shows the application potential of microwave technique in SOFC manufacturing.

2. Experimental

2.1. Cell fabrication

Mechanically mixed NiO powder and YSZ powder (AGC Seimi Chem. Corp., Japan) were used to prepare NiO–YSZ anode substrate pellets. The powders were mixed at a ratio of 60:40 vol%. In order to maintain a sufficiently porous structure, 10 wt% organic pore former was added to the powder mixture. The final mixed powder was uniaxial compressed in a metal die at 150 MPa pressure to make anode substrate pellets with a diameter of 20 mm and a thickness of 0.7 mm. The pellets obtained were then pre-sintered at 1200 °C for 2 h in a conventional sintering furnace to improve the mechanical strength.

Microwave susceptor pellets were prepared before the microwave sintering experiments. The microwave susceptor pellets (30 mm in diameter, and 3 mm in thickness) were made by the same technique as substrate pellets, while the material used is $72.5ZnO–27MnO_2–0.5Al_2O_3$ (ZMA, hereafter). ZMA was prepared by mixing zinc oxide, manganese dioxide and alumina powders (High Purity Chemical Laboratory, Japan) [3]. Spacer pellets (20 mm in diameter, and 0.8 mm in thickness) were made by die-pressing YSZ powder (0.3 μm, Tosoh Co., Japan) and then sintered in furnace at 1350 °C for 2 h. The spacers were used between the cell and the ZMA susceptor to prevent contamination.

The thin film electrolyte was dip-coated onto the substrate pellets. The coating slurry was prepared by YSZ (8 mol% yttria stabilized zirocnia) powder (Tosoh Co., Japan). A mixture of isopropyl alcohol and terpineol was used as solvent, while ethyl cellulose was used as an organic binder. The organic binder was mixed with YSZ powder first, then added into the solvent. The slurry was ball-mixed for 24 h to obtain a homogeneous slurry, which contains 0.33 g solid per micro liter slurry.

After dip-coating, the pellets were dried in the air for 24 h, and then divided into two groups. The coated pellets in the first group were sintered in a multimode domestic microwave oven (SHARP, RE-T31, 700 W). The anode substrate pellet was sandwiched by two YSZ spacer pellets and then they were sandwiched by another two ZMA susceptor pellets. The pellets series was then put into a fibrous alumina-silica case (Kaowool 1700 Board, Isolite Insulating Products Co. Ltd., Japan) for thermal insulation. The insulation case was then put at the center of the turning table with a kaowool board as spacer between the case and the glass table. The power was turned to 700 W and the cell was sintered for 10 min and then cooled down for 1 h at room temperature. The coated pellets in the second group were sintered in conventional thermal heating oven (MSTR16-430) at 1400 °C for 3 h, with the temperature heating up and cooling down rate at 10 °C min^{-1}, as standard reference cells.

Pure $La_{0.8}Sr_{0.2}MnO_x$ (LSM) powder (0.4 μm) was used as cathode material in this study. The powder was then mixed with the terpineol solvent and the ethyl-cellulose binder in agate mortar to obtain cathode printing paste. The LSM paste was then screen-printed onto electrolyte film for the two groups. The first group with cathode printed was sintered in microwave oven for 10 min, with an effective area of 28.26 mm^2. For cathode sintering, only one ZMA susceptor with one YSZ spacer was applied as the sintering base to reduce the sintering temperature. The second group was sintered at 1150 °C for 3 h, with the temperature heating up and cooling down rate at 3.3 °C min^{-1}.

2.2. Cell performance measurement devices

The SOFC performance measurement setup is shown in Fig. 1. Pt meshes was used as current collectors, which were pressed against the electrodes of the cell by mechanical force. Glass rings were used as the gas seals between two outer alumina tubes, and the two outer tubes were also pressed against the cell by spring. After the temperature was increased beyond 600 °C, the glass seals melted and resulted in perfect gas sealing. The performance of SOFC was evaluated at different temperatures by introducing humidified H_2 to anode as fuel, and pure oxygen to cathode as oxidant. For both hydrogen and oxygen, the gas flow rates were kept at 50 sccm. *I–V* characterization and anode–cathode (A–C) impedance (frequency range 1–10^6 Hz, AC signal stength 10 mV) measurements were con-

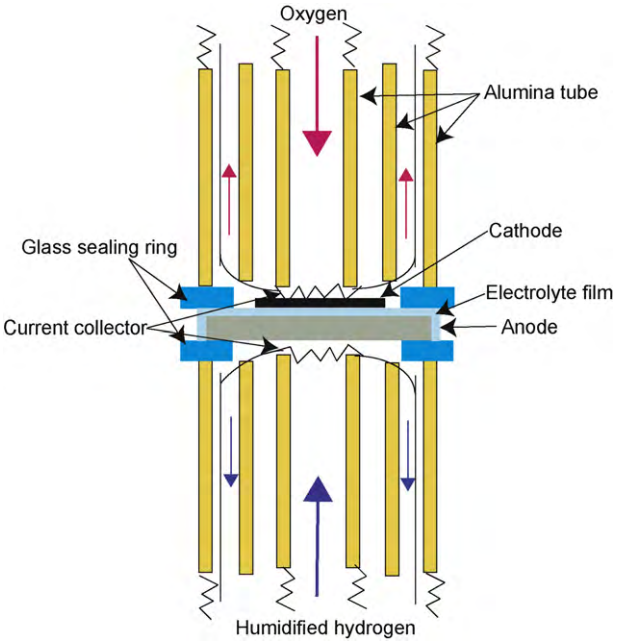

Fig. 1. Schematic diagram of SOFC measurement setup.

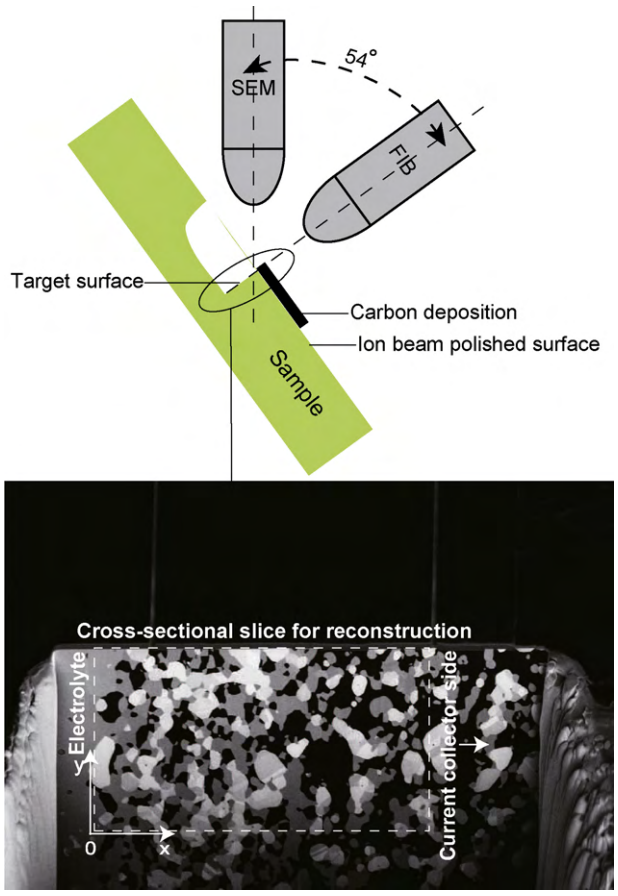

Fig. 2. Schematic diagram of FIB-SEM setting.

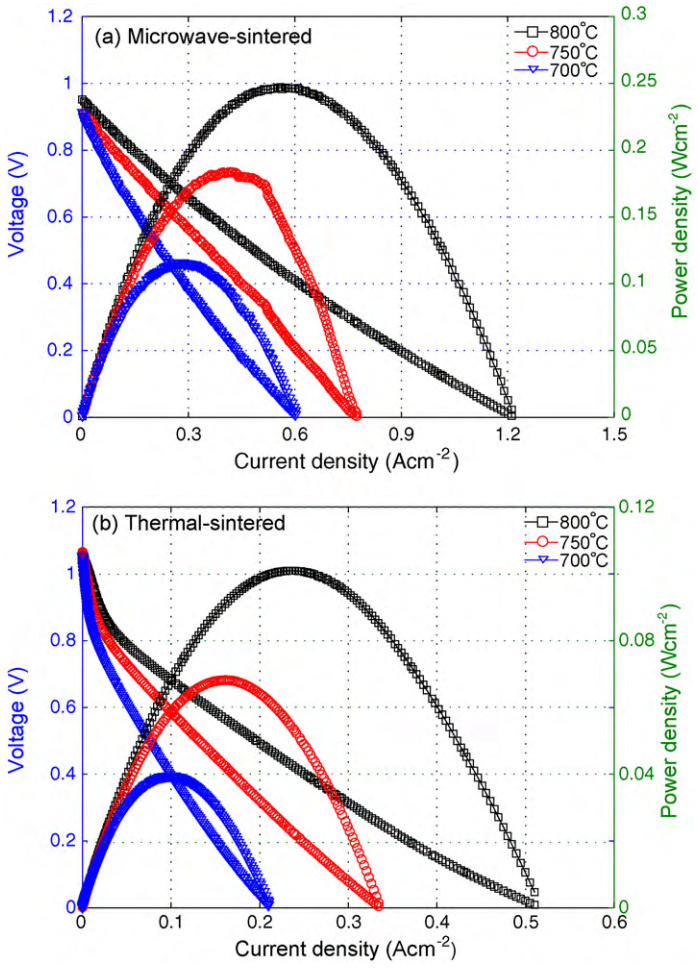

Fig. 3. The *I–V* characteristics comparison between microwave-sintered and thermal-sintered anode support SOFC at different temperatures. 3% H_2O, 97% H_2 as fuel and 100% oxygen as oxidant.

ducted with a Solartron frequency analyzer (1255B) and a Solartron interface.

2.3. Image processing and 3-D reconstruction

Image observation and quantification of the sample microstructures after measurements were facilitated by FIB-SEM (Carl Zeiss, NVision 40, Germany). The system is equipped with Gemini FE-SEM column, zeta FIB column and a multi-channel gas injection system (SIINT). 3-D microstructures of both anode and cathode can be virtually reconstructed in a computional field by using 2-D SEM images obtained through the FIB-SEM observation, which is shown in Fig. 2 [8,9]. Cross-section of the observed sample was first polished by Ar-ion beam cross-section polisher (JEOL Ltd., SM-09010, Japan), which results in less damage and smoother cross section compared to the diamond slurry polishing. A layer of carbon was then deposited onto polished surface to indicate the reconstructed region. All the 2-D images were processed in software Matlab for the subsequent reconstruction of 3-D structure in software Avizo (Maxnet Co. Ltd., Japan). The quantitative comparison between microwave-sintered and thermal-sintered cells was based on their corresponding 3-D reconstruction.

3. Results and discussion

3.1. Experimental results

Fig. 3 shows the comparison of *I–V* performances between microwave-sintered and conventional thermal-sintered cells. It is shown that the maximum power densities are 0.12, 0.18 and 0.25 W cm^{-2} for microwave-sintered cell and 0.04, 0.07 and 0.11 W cm^{-2} for thermal-sintered cells at 700, 750 and 800 °C, respectively. The anode–cathode open circuit potential of microwave-sintered cell is around 0.95 V, which is lower than the theoretical value 1.14 V. The lower open circuit potential indicates the possibility of certain leakage across the thin YSZ film, which is caused by micro-cracks formed in the ultra-fast microwave sintering process. Besides, the non-uniform electromagnetic field within domestic microwave oven may also lead to the micro-cracks within non-uniform sintering process [7]. Without gas leakage problem, the performance of microwave-sintered cell can be further improved.

Fig. 4 shows the comparison of anode–cathode impedance spectra between microwave-sintered and conventional thermal-sintered cells. According to the high frequency spectra, the ohmic resistance of the cell sintered by microwave was about 0.05 Ω cm^2 at 800 °C which is only half of thermal-sintered cell. With the increase of temperature, the ohmic resistance slightly increases in both cases. From 800 to 700 °C, for microwave-sintered cell, the electrode polarization increases from 0.5 to 1 Ω cm^2, while for thermal-sintered cell, the increase is from 5.5 Ω cm^2 to about 30.5 Ω cm^2. Both of the impedance changes indicate that low-frequency polarization dominates the cell performance, especially for thermal-sintered cell. The initial electrochemical behavior of pure LSM cathode has been studied by Jiang and co-worker [10] at 900 °C, which showed that pure LSM always presented very high activation polarization in the initial state (5.5 Ω cm^2), which is close

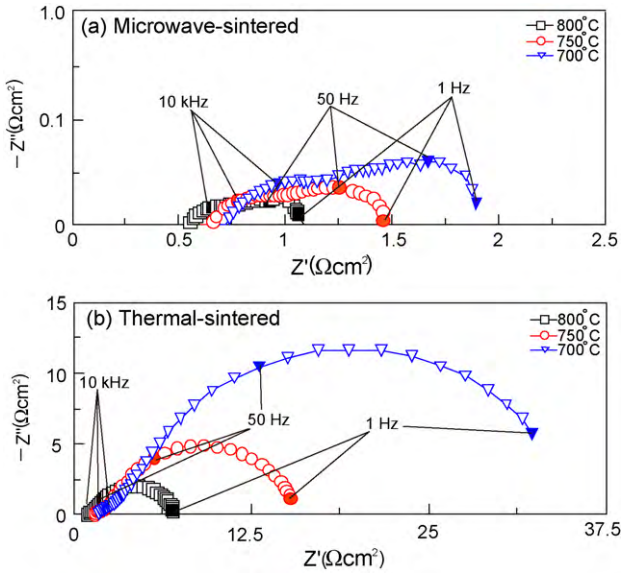

Fig. 4. Anode to cathode impedance spectra comparison in OCV between microwave-sintered and thermal-sintered cells.

to our data. After 3 h cathodic current passage of 0.2 A cm^{-2}, the interface polarization was reduced to 2.1 Ω cm^2. For microwave-sintered cell, much smaller activation polarization (0.5 Ω cm^2) was obtained at 800 °C.

The microstructures of the cells after testing were examined by SEM. Fig. 5 shows the SEM images of cross-sections, and the top surfaces of anodes, electrolytes and cathodes for both microwave-sintered and thermal-sintered cells. From the comparison it can be observed that, with the same materials used, microwave sintering results in very different microstructures from thermal sintering method. After sintering, microwave-sintered cell remained flat while thermal-sintered one was bent. Several cells were tested, and similar deformations were obtained. For anode, microwave sintering method produces finer and sharper particles than thermal sintering. For cathode, microwave sintering produced coarser LSM particle than thermal sintering. Certain amount of sub-micron particles was distributed uniformly on the LSM particle surface.

3.1.1. 3-D reconstructions

Fig. 6 shows the 2-D slice images of microwave-sintered and thermal-sintered anode and cathode cross-sections. Based on series of sliced images, anode and cathode can be reconstructed in 3-D [8]. It is obviously observed that microwave sintering results in more dense and finer composite anode microstructure and much coarser particle for cathode. Fig. 7 shows the 3-D reconstruction of the microstructures for both microwave-sintered and thermal-sintered anodes, with separated Ni and YSZ phases. In the reconstructions, *x* and *y* axis have been indicated in Fig. 2 and *z* axis is perpendicular to *x*–*y* plane along which image slices are subsequently aligned. Non percolated clusters in both Ni and YSZ networks are shown in red color. The connectivities of both Ni and YSZ phases networks are measured by the volume percentage of the percolated cluster. The microstructural parameters are summarized in Table 1. From the comparison, it can be seen that, with a much shorter sintering time and lower sintering temperature [3], microwave sintering method produces more dense composite anode structure with better phase connections for both Ni and YSZ.

In order to further investigate the anode microstructural differences between microwave sintering and thermal sintering methods, TPB networks corresponding to Fig. 7 was reconstructed as shown in Fig. 8. Centroid method was used to calculate the TPB densities [11]. TPB density is defined as the length of TPB within unit volume. The total TPB densities and active TPB densities in different directions for both cells are listed in Table 2. It is shown that microwave sintering results in larger total TPB density than thermal sintering, which is due to finer particle size. Only active TPB, which connects current collector to electrolyte, contributes to cell performance. The active TPB densities along three axis directions are nearly the same, which means that both microwave sintering and thermal sintering produce isotropic anode microstructures. The active TPB density takes possession of 78% of the total density for microwave-sintered anode and 72% for thermal-sintered anode. The higher total TPB density and active TPB density of microwave-sintered anode can partially explain the better performance and lower polarization of microwave-sintered cell.

Fig. 9 shows the 3-D reconstructions of microwave-sintered and thermal-sintered cathodes. The corresponding porosities for two cathodes are shown in Table 1. It is evident that microwave sintering results in much coarser LSM particle than thermal sintering. This can be explained by the higher sintering temperature and non-thermal driving force, which can enhance thermal sintering [5]. For pure LSM cathode, TPB concentrates at the interface between cathode and electrolyte and the 2-D TPB densities of two cells are shown in Table 2. It is seen that thermal sintering leads to more than twice TPB density than microwave sintering method, which can not explain the better performance of the microwave-sintered cell. Jiang et al. [12,13] proved that the initial large polarization behavior of freshly prepared LSM cathode is originated from the enrichment of passivation species such as SrO and MnO_x on the LSM particle surface layer. SrO and MnO_x could occupy the active sites and inhibit the surface dissociation and diffusion of oxygen. Cathodic polarization as well as acid etching has been proved to be able to effectively remove or decrease the passivation species from the active sites on LSM surface. The significant improvement of the initial cathode performance caused by the two methods have been proven to reduce the initial cathodic polarization to less than one tenth of the original value, with constant TPB density. Lee et al. [14] investigated the active reaction sites for oxygen reduction in LSM/YSZ electrodes. Surface oxide vacancies as well as the TPB sites are active in oxygen reduction process. TPB sites are favored since additional diffusional processes are required for the former sites. At lower oxygen pressure, the TPB dominates the surface reaction while the contribution from the surface sites becomes more important at higher oxygen pressure (1 atm). With high oxygen pressure, surface grain boundary diffusion in porous electrode can not be ignored for its contribution to oxygen reduction, since diffusion in grain boundary is much faster than bulk diffusion. Adler [15] summarized the factors governing oxygen reduction in SOFC cathode. The cathode performance is limited by at least four physical processes: adsorption of oxygen, ambipolar diffusion (defined as the diffusion of positive and negative particles in a plasma at the same rate due to their interaction via the electric field) transport to solid–solid interface, interfacial electrochemical kinetics and ionic transport in the ionic sub-phase, among which TPB density can only dominate the interfacial electrochemical kinetics. With high oxygen pressure, the other three process may become the rate-

Table 1
Microstructural properties comparison between microwave-sintered and thermal-sintered cells based on 3-D reconstruction.

Parameters	Microwave-sintered	Thermal-sintered
Anode porosity	34.1%	39.7%
Ni percolation percentage	96.2%	93.4%
YSZ percolation percentage	98.9%	98.0%
Cathode porosity	36.5%	45.0%

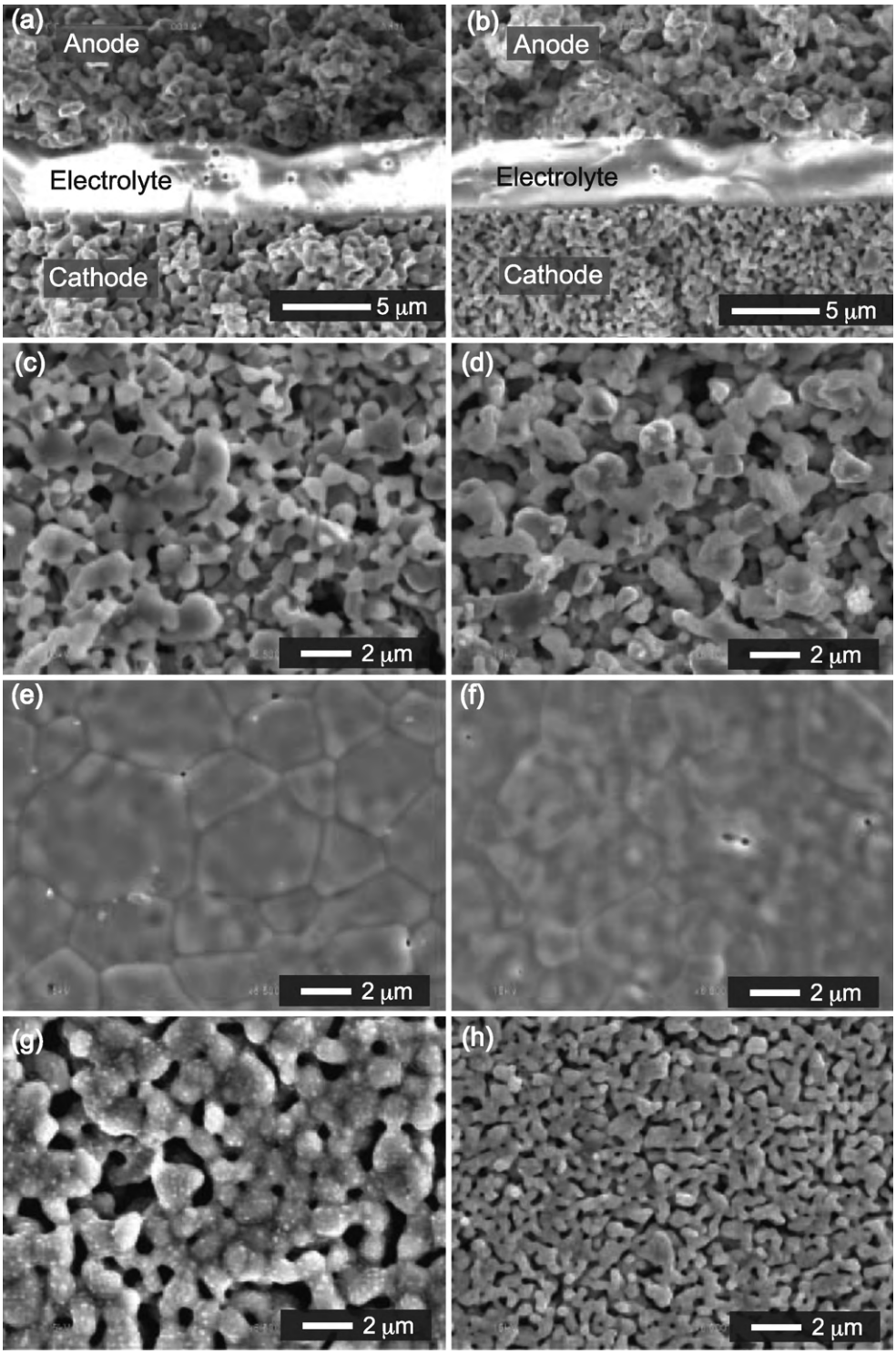

Fig. 5. SEM images of (a) microwave-sintered, (b) thermal-sintered cell cross-section, (c) microwave-sintered, (d) thermal-sintered anode, (e) microwave-sintered, (f) thermal-sintered electrolyte, (g) microwave-sintered and (h) thermal-sintered cathode.

determine process and dominate the cathode performance with TPB density. In microwave sintering, the non-thermal effect may result in crystal structure change to the material and influence the final performance of cathode. In our experiments, oxygen inlet pressure was set at 1 atm, which means that grain boundary of LSM also contributes to the cathodic oxygen reduction process, which may even dominate the cathode performance. Even with lower 2-D TPB density at cathode–electrolyte interface, microwave-sintered cathode can show better performance if the concentration of the active surface sites is higher.

In microwave sintering, once the material is heated to a critical temperature via susceptor, the material can be self-heated. Above the critical temperature, the ionic mobility becomes large enough for the ceramic ions near surface layer to absorb microwave energy and causes dielectric loss due to the ionic movement. Microwave then can interact with ceramic surface through either surface polar-

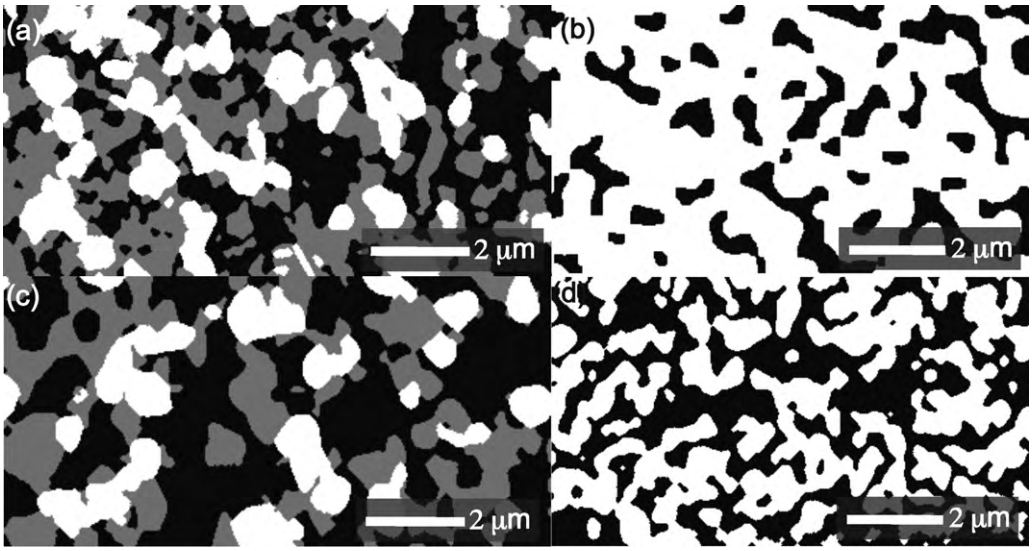

Fig. 6. Cross-sectional slice of microwave-sintered (a) anode, (b) cathode and thermal-sintered, (c) anode and (d) cathode for 3-D reconstruction. White color indicates Ni phase, grey color indicates YSZ phase and black color indicates pore for the electrode.

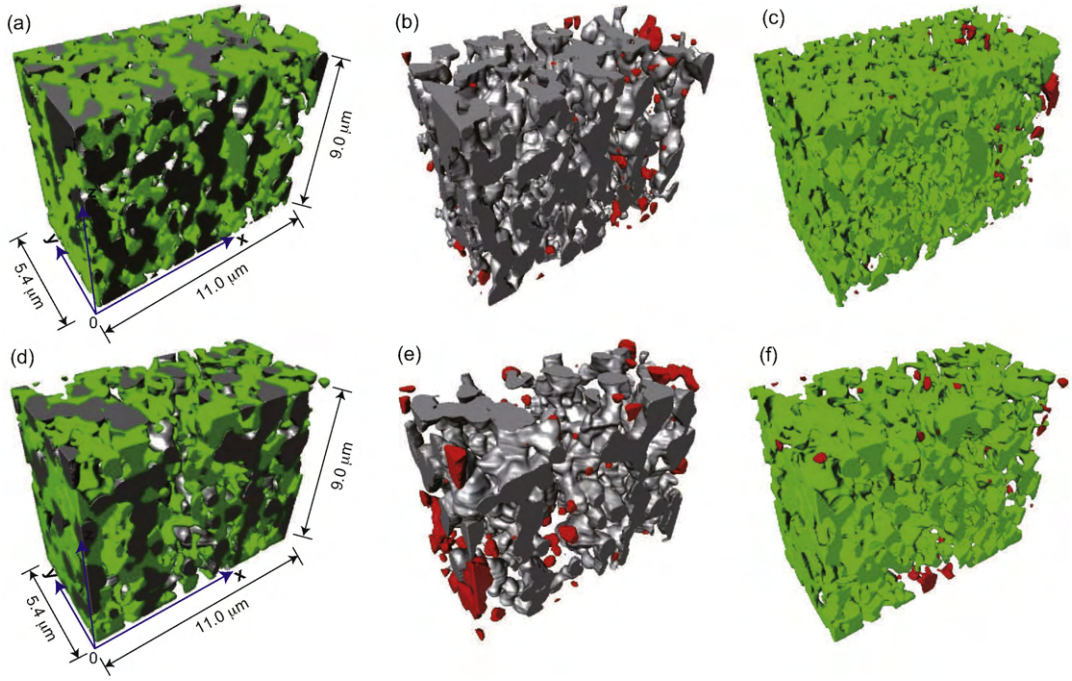

Fig. 7. 3-D reconstructions of microwave-sintered (a) composite anode, (b) Ni phase, (c) YSZ phase and thermal-sintered, (d) composite anode, (e) Ni phase and (f) YSZ phase. Red color indicates the non-percolated particle clusters separated from the main phase network. (For interpretation of the references to color in this figure legend, the reader is referred to the web version of the article.)

ization or conduction processes driven by ponderomotive force (F_p) [5,16]. In microwave driving surface polarization process, the high frequency ion oscillation results in microwave-excited ion current which may result in similar effects as normal electrical current passing through LSM in cathodic polarization. The initial large cathode polarization then can be reduced by microwave driving surface polarization. For the conduction process of mobile ions, ponderomotive force is then defined. Ponderomotive force is defined as a nonlinear force that a charged particle experiences in an inhomogeneous oscillating electromagnetic field [17], which is expressed as,

$$F_p = -\frac{e^2}{4m\omega^2}\Delta E^2 \quad (1)$$

where e is the electrical charge of the particle, m is the ion mass, ω is the angular frequency of oscillation of the field, and E is the amplitude of the electric field. This equation shows that a charged particle in an inhomogeneous oscillating field not only oscillates at the frequency but also drifts toward the weak field area. It is known that the sign of the particle charge does not change the direction of the ponderomotive force. Ponderomotive force is thus an electromagnetic force, which is able to move mass. Microwave presents the largest amplitude at ceramic surface and dissipate to zero into the ceramic bulk with a depth of nanometer scale [17]. In the interacting process, all kinds of mobile ions at ceramic surface experience a relatively large ponderomotive driving force towards the ceramic bulk. With this mechanism, continuing crystal vacancies are driven towards the ceramic surface in an opposite direction.

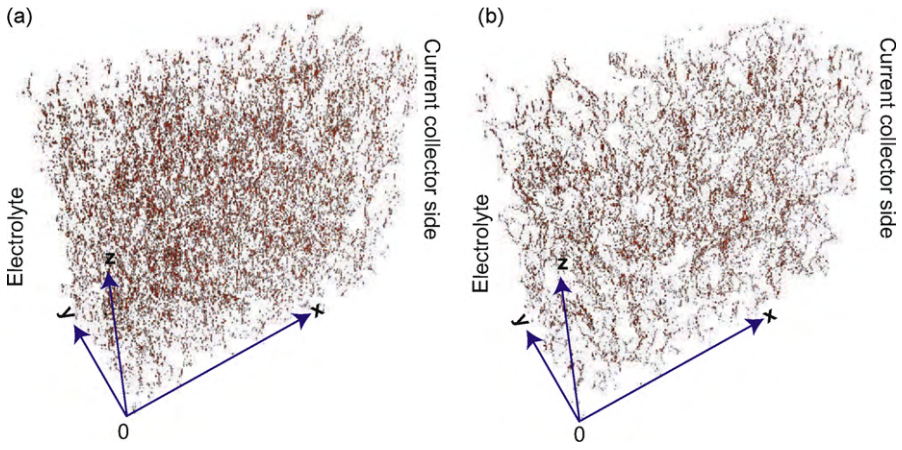

Fig. 8. 3-D reconstructions of TPB networks for (a) microwave-sintered anode and (b) thermal-sintered anode corresponding to Fig. 7.

Table 2
TPB network properties of microwave-sintered and thermal-sintered anodes.

TPB density	Microwave-sintered ($\mu m\,\mu m^{-3}$)	Thermal-sintered ($\mu m\,\mu m^{-3}$)
Anode (3-D)		
Total TPB density	5.36	4.02
Active TPB density ($x = 0 \rightarrow 11.0\ \mu m$ direction)	4.15	2.89
Active TPB density ($y = 0 \rightarrow 5.4\ \mu m$ direction)	4.15	2.90
Active TPB density ($z = 0 \rightarrow 9.0\ \mu m$ direction)	4.12	2.91
Active TPB density ($x = 11.0 \rightarrow 0\ \mu m$ direction)	4.10	2.93
Active TPB density ($y = 5.4 \rightarrow 0\ \mu m$ direction)	4.15	2.96
Active TPB density ($z = 9.0 \rightarrow 0\ \mu m$ direction)	4.17	2.89

TPB density	Microwave-sintered ($\mu m\,\mu m^{-2}$)	Thermal-sintered ($\mu m\,\mu m^{-2}$)
Cathode (2-D)		
Total TPB density	1.7	4.0

The increasing concentration of vacancy may create more active oxygen adsorption sites on LSM surface and then reduce the initial cathodic polarization. At the same time, microwave induced vacancy movement at high temperature may also enhance the thermal sintering process, which leads to much coarser microstructure in a short sintering time.

In order to prove the improvement of LSM cathode in microwave sintering, another experiment was conducted. A thermal-sintered cell was sintered again in microwave with one-side susceptor and spacer used. The cell impedances comparison between the thermal-microwave-sintered cell and thermal-sintered cell is shown in Fig. 10. From the comparison, it is obvious that cell polarization is reduced compared to the initial thermal-sintered cell, which proves that microwave sintering process have the similar effect as current passage in cathodic polarization process. The lower sintering temperature with one-side susceptor make it reasonable to ignore the microwave sintering influence on anode side. The SEM image of thermal-microwave-sintered cathode and purely thermal-sintered cathode are compared in Fig. 11. The thermal-microwave-sintered cathode presents coarser microstructure with a state in between microwave-sintered and thermal-sintered cathodes. The coarsening of cathode proves that TPB does not dominate the cell performances, but the surface active sites.

Besides the initial performances, the cell durabilities have been tested for both cells. Microwave-sintered cell showed very stable performance in a 140 h discharging process while thermal-sintered one showed unstable performance and even sudden failing at 20 h.

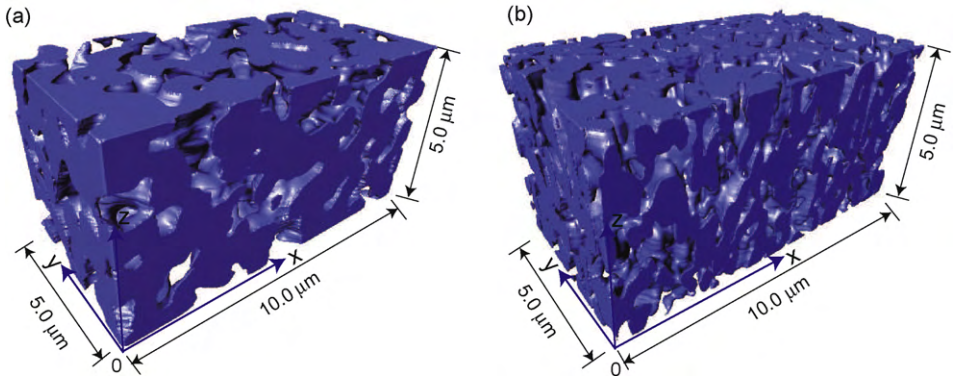

Fig. 9. 3-D reconstructions of (a) microwave-sintered cathode and (b) thermal-sintered cathode.

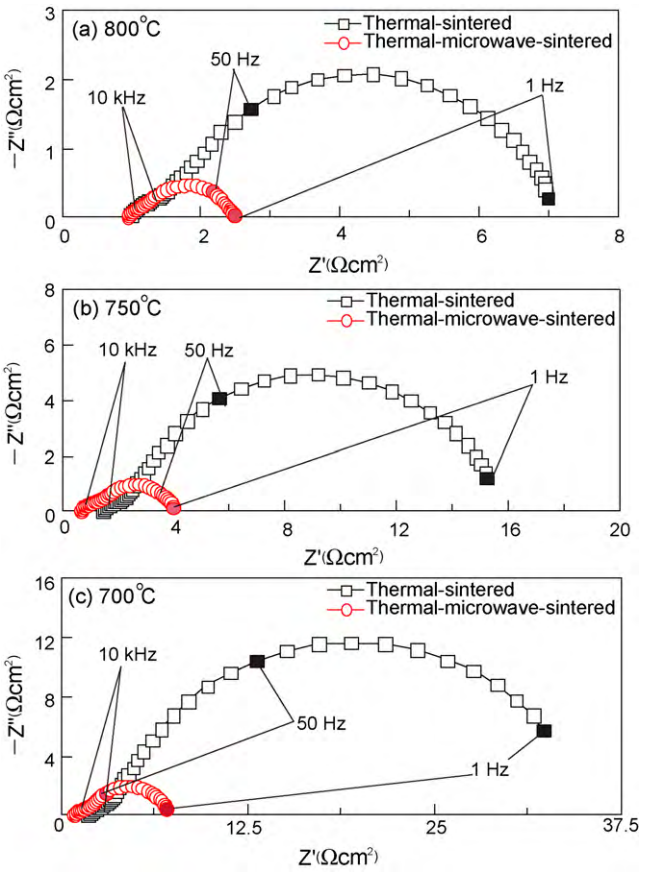

Fig. 10. Thermal-sintered cell anode to cathode impedance spectra in OCV before and after microwave treatment.

Details of the durability tests will be shown in the next paper. In the future, specially designed microwave oven can be used for fabricating planar anode support SOFC to improve the cell quality and meet all the practical manufacturing requirements, such as heating program, SOFC size, materials and so on. With uniform electromagnetic field and controllable power output, the gas leakage problem can be solved. For the cell fabricated by thermal sintering, it can also be processed in microwave to improve the cathode performance. Further investigation should be conducted to explain the advantages of microwave sintering in cathode fabrication.

4. Conclusions

Anode support SOFCs were fabricated by both microwave-sintering and conventional thermal-sintering methods. The cell performances in the intermediate temperature range of 700–800 °C were measured for both cells. Microwave-sintered cell shows higher initial performance and lower polarization than thermal-sintered one. The reconstructed 3-D structures were used to quantify anode and cathode microstructural parameters such as porosity, percolation percentage and TPB densities. With a much shorter sintering time, microwave sintering results in finer and sharper particles and higher TPB densities in anode, but coarser particles and lower TPB density in cathode. The higher cell performance is partially explained by the finer anode microstructure and the non-thermal effect in the microwave sintering of cathode. The non-thermal effect in microwave sintering of cathode is caused by the enhancement of active surface sites for oxygen adsorption, which is caused by the polarization effect of ponderomotive force. With ultra-fast sintering process and much lower cathodic polarization, microwave can be applied in SOFC manufacturing as a new technique with much higher efficiency compared to conventional sintering process.

Acknowledgments

This work was supported by the New Energy and Industrial Technology Development Organization (NEDO) under the Development of System and Elemental Technology on Solid Oxide Fuel Cell (SOFC) Project.

References

[1] S.P.S. Badwal, M.J. Bannister, R.H.J. Hannink, Science and Technology of Zirconia V, Technomic Publishing Company, 1993.
[2] Y. Zhang, X. Huang, Z. Lu, Z. Liu, X. Ge, J.X.X. Xin, X. Sha, W. Su, J. Am. Ceram. Soc. 89 (2006) 2304–2307.
[3] S. Fujitsu, M. Ikegami, T. Hayashi, J. Am. Ceram. Soc. 8 (2000) 2085–2087.
[4] M.A. Janney, C.L. Calhoun, H.D. Kimrey, J. Am. Ceram. Soc. 2 (1992) 341–346.
[5] D.E. Clark, Annu. Rev. Mater. Sci. 26 (1996) 299–331.
[6] E.O. Oh, H. Kim, D.C. Baek, J. Park, H.-R. Kim, J.-H. Lee, H.-W. Lee, C.M. Whang, J.-W. Son, ECS Trans. 7 (2007) 743–748.
[7] Z. Jiao, N. Shikazono, N. Kasagi, J. Power Sources 195 (2009) 151–154.
[8] H. Iwai, N. Shikazono, T. Matsui, H. Teshima, M. Kishimoto, R. Kishida, D. Hayashi, K. Matsuzaki, D. Kanno, M. Saito, H. Muroyama, K. Eguchi, N. Kasagi, H. Yoshida, J. Power Sources 195 (2010) 955–961.
[9] J.R. Wilson, J.S. Cronin, A.T. Duong, S. Rukes, H.-Y. Chen, K. Thornton, D.R. Mumm, S. Barnett, J. Power Sources 195 (2010) 1829–1840.
[10] Y.D. Zhen, S.P. Jiang, J. Electrochem. Soc. 12 (2006) A2245–A2254.

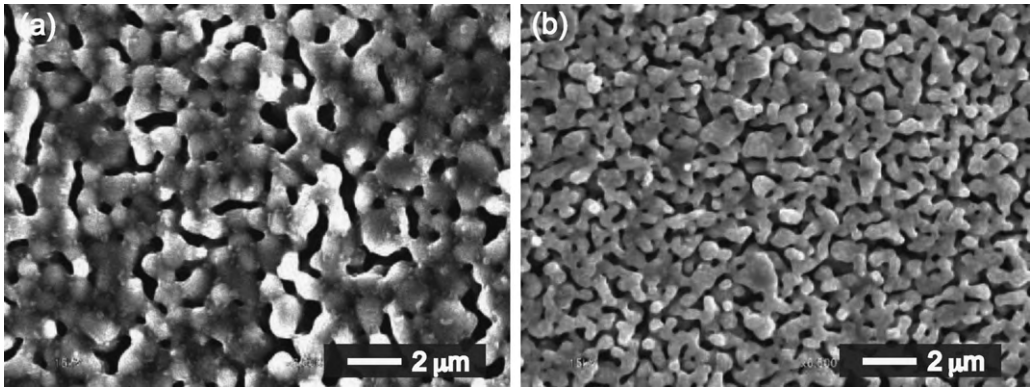

Fig. 11. (a) Thermal-microwave-sintered cathode and (b) thermal-sintered cathode.

[11] N. Shikazono, D. Kanno, K. Matsuzaki, H. Teshima, S. Sumino, N. Kasagi, Numerical Assessment of SOFC Anode Polarization Based on Three-Dimensional Model Microstructure Reconstructed from FIB-SEM Image, J. Electrochem. Soc. 157 (2010) B665–B672.
[12] S.P. Jiang, J.G. Love, J.P. Zhang, M. Hoang, Y. Ramprakash, A.E. Hughes, S.P.S. Badwal, Solid State Ionics 121 (1999) 1–10.
[13] S.P. Jiang, J.G. Love, Solid State Ionics 138 (2001) 183–190.
[14] H.Y. Lee, W.S. Cho, S.M. Oh, H.D. Wiemhofer, W. Gopel, J. Electrochem. Soc. 142 (1995) 2659–2664.
[15] S.B. Adler, Chem. Rev. 104 (2004) 4791–4843.
[16] J.H. Booske, R.F. Cooper, S.A. Freeman, K.I. Rybakov, V.E. Semenov, Phys. Plasm. 5 (1998) 1664–1670.
[17] S.A. Freeman, J.H. Booske, R.F. Cooper, J. Appl. Phys. 83 (1998) 5761–5772.